LA-UR-97-3787, LANL, Los Alamos (1997);
to be published in *Nucl. Instr. Meth. A*

Experimental and computer simulation study of the radionuclides produced in thin ^{209}Bi targets by 130 MeV and 1.5 GeV protons

Yu.E. Titarenko [a,*], O.V. Shvedov[a], M.M. Igumnov[a], R. Michel[b], S.G. Mashnik[c,f], E.I. Karpikhin[a], V.D. Kazaritsky[a], V.F. Batyaev[a], A.B. Koldobsky[d], V.M. Zhivun[d], A.N. Sosnin[e], R.E. Prael[f], M.B. Chadwick[f], T.A.Gabriel[g], M. Blann[h]

[a] *SSC Institute for Theoretical and Experimental Physics, B. Cheremushkinskaya 25, Moscow, 117259, Russia*
[b] *Center for Radiation Protection and Radioecology, University Hannover, Am Kleinen Felde 30, D-30 167 Hannover, Germany*
[c] *Bogoliubov Laboratory of Theoretical Physics, JINR, Dubna, Moscow Region, 141980, Russia*
[d] *Moscow Engineering Physical Institute, Moscow, 115409, Russia*
[e] *Laboratory of Computing Technique and Automation, JINR, Dubna, Moscow Region, 141980, Russia*
[f] *Los Alamos National Laboratory, Los Alamos, NM 87545, USA*
[g] *Oak Ridge National Laboratory, Oak Ridge, TN 37831, USA*
[h] *7210E Calabria ct, San Diego, CA 92122, USA*

Abstract

The results of experimental and computer simulation studies of the yields of residual product nuclei in ^{209}Bi thin targets irradiated by 130 MeV and 1.5 GeV protons are presented. The yields were measured by direct high-precision γ-spectrometry. The γ-spectrometer resolution was 1.8 keV in the 1332 keV line. The γ-spectra were processed by the ASPRO code. The γ-lines were identified, and the cross sections defined, by the SIGMA code using the GDISP radioactive database. The process was monitored by the ^{27}Al(p,x)^{24}Na reaction. Results are presented for comparisons between the ^{209}Bi(p,x) reaction yields obtained experimentally and simulated by the HETC, GNASH, LAHET, INUCL, CEM95, CASCADE, and ALICE codes.

*Corresponding author. Tel.: +7 095 125 9100, fax: +7 095 127 0543, e-mail: titaren@vitep5.itep.ru

1. Introduction

Ecology has become a matter of priority in all of the developed countries. Utilization and management of wastes from nuclear power plants is a priority among the environmental protection measures. Besides, the nations that posses nuclear weapons have become concerned with disposal or peaceful uses (conversion) of surplus weapon plutonium and of highly-enriched uranium. Appropriate approaches are under development in Europe, North America, Japan, and Russia [1, 2, 3, 4].

In practice, two basic approaches are under study, namely, the safe long-term storage of long-lived radioactive wastes, which postpones the need for destroying the wastes, and nuclear transmutation, which turns the wastes into stable and shorter-lived nuclides. Some methods that combine the two approaches are also being developed.

The concept of accelerator-driven electronuclear facilities was suggested some four decades ago [5] and developed persistently ever since is considered to be a promising technology for waste transmutation. Such facilities differ from conventional nuclear power facilities that are operated in critical mode supported by delayed neutrons. An accelerator provides the neutrons to sustain a chain fission reaction, so that such facilities are subcritical. The neutron source is a nucleon-meson cascade initiated by 0.8-2.0 GeV protons that strike a target located inside the facility. In terms of neutron yield, nonfissible Pb, Bi, W, and Hg, as well as fissible U and Th, are most suitable as target materials. Composite targets with a suppliment of the long-lived ^{99}Tc and ^{90}Sr fission products may also be interesting.

The neutron-generating target provides a neutron flux that is sufficient for effective transmutation to occur in a neutron-multiplying blanket that contains nuclear fuel and long-lived nuclear wastes.

The accelerator-driven facilities are advantageous mainly because of their subcritical mode of operation, thus precluding any emergencies accompanied by an uncontrollable rise of power. This is primarily due to the possibility for proton accelerators to be controlled, or else de-energized promptly, so that the power of the facility blanket falls completely.

Current development of neutron-generating targets for accelerator-driven nuclear facilities is aimed at extending the data on the numerous reactions induced by high-energy neutrons and protons in target materials, including generation of product nuclei within the range of atomic numbers A from 1 up to the target atomic number plus 1. The generated nuclei may be both radioactive and stable. Their nuclear characteristics may affect the rated performances and safe operation of a facility through:

- total activity of the target,
- "poisoning" the target,
- accumulation of long-lived radionuclides to be transmuted,
- alpha-activity of the isotopes (e.g., Po) produced,
- production of nuclides with a high vapor pressure (T, He, Hg, etc.),
- accumulation of chemically-active nuclides, thus reducing the corrosion resistance of the structure materials.

The present-day accuracy requirements of predicting the yields of product nuclei are estimated to be about 30% [6]. The major difficulty is that experiments with heavy target nuclei can only detect from 80 to 100 product nuclei, whereas the actual nuclide production yields are an order of magnitude higher. It has been estimated that only 300-400 of the long-lived nuclides are of interest, so we have to use mainly the theoretically-predicted reaction cross sections. The predictive power of the computational methods and of the respective computer simulation codes can be improved by making comparisons with the still scanty available experimental data [7, 8]. In his review of nuclide yield data, A.J. Koning [6] has shown that the NSR and EXFOR databases are insufficient at energies above 20 MeV.

With the above approach, the accuracy requirements may be met by step by step improvements in the computer simulation of intranuclear processes, as well as by extending the experimental data base, in particular the data on the nuclide yields in thin targets irradiated by up to 2 GeV protons. A comprehensive comparison between the codes and the experimental data is expected to help determine the ranges of energies and mass numbers described most adequately by the codes. In the given work the energy choice is caused by the presence in a target proton spectrum of two basic components which actively participate in secondary nuclides formation: the primary one, with energy 1-2 GeV, created directly due to protons in the accelerator beam; and a secondary one, with energy basically up to $\sim$ 0.2 GeV, formed in primary proton interactions with target nucleus.

2. Techniques

Generation of residual product nuclei in proton interactions with a target nucleus is due to the intranuclear processes of spallation, fission, fragmentation, and evaporation of light nuclei and nucleons. The general form of proton interactions with a target nucleus is

$$ {}^{A_T}_{Z_T}T(p,x){}^{A}_{Z}N \ , \tag{1} $$

where, as usual, (p,x) designates a nuclear reaction type, T and N are chemical symbols of the elements, i.e. of the target nucleus and of product nuclei, A_T and Z_T are respectively the mass number and the charge of a target nuclide, A and T are respectively the mass number and the charge of a nuclide produced in the respective nuclear reaction.

The present work determines the independent and cumulative yields of radioactive nuclear reaction products. The $^{27}Al(p,x)^{24}Na$ reaction is used as monitor.

The variations in the concentrations of two "congener" nuclides produced in a thin target under irradiation may be presented as

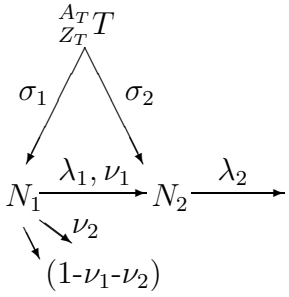

$$\begin{cases} \dfrac{dN_1}{dt} = \sigma_1 N_T \Phi - \lambda_1 N_1 \ , \\ \dfrac{dN_2}{dt} = \sigma_2 N_T \Phi + \nu_1 \lambda_1 N_1 - \lambda_2 N_2 \ , \end{cases} \tag{2}$$

with the initial conditions $N_1(0) = 0$ and $N_2(0) = 0$. Here, N_1 and N_2 are the numbers of nuclei produced, σ_1 and σ_2 are their yields, λ_1 and λ_2 are the decay constants, ν_1 and ν_2 are the probabilities for nuclide 1 to decay into nuclide 2 and 3, i.e. the branching factors, N_T is the number of ${}^{A_M}_{Z_M}T$ in an experimental sample, Φ is the proton flux and t is the current time. In the case of a pulsed irradiation mode, then, the solution for the set of differential equations (2) is described by the expressions

$$N_1\left[(K-1)T+\tau\right] = \frac{N_T \Phi \sigma_1 F_1}{\lambda_1} \ , \tag{3}$$

$$N_2\left[(K-1)T+\tau\right] = N_T \Phi \nu_1 \frac{1}{\lambda_2 - \lambda_1}\sigma_1 F_1 + \frac{N_T \Phi}{\lambda_2}\left[\sigma_2 - \frac{\lambda_1}{\lambda_2 - \lambda_1}\nu_1 \sigma_1\right] F_2 \ , \tag{4}$$

where τ is the duration of a single proton pulse, T is the pulse repetition period, K is the number of irradiation pulses, and

$$F_i = \left(1 - e^{-\lambda_i \tau}\right) \frac{1 - e^{-\lambda_i K T}}{1 - e^{-\lambda_i T}} \ , \qquad i = 1, 2, Na \ .$$

The after-irradiation decay of the nuclides produced is described by the set

$$\begin{cases} \dfrac{dN_1}{dt} = -\lambda_1 N_1 \ , \\ \dfrac{dN_2}{dt} = \nu_1 \lambda_1 N_1 - \lambda_2 N_2 \ . \end{cases} \tag{5}$$

The solution for (5) is

$$N_1(t) = N_{1_0} e^{-\lambda_1 t} \ , \tag{6}$$

$$N_2(t) = \left[N_{2_0} + \frac{\lambda_1}{\lambda_1 - \lambda_2}\nu_1 N_{1_0}\right] e^{-\lambda_2 t} - \frac{\lambda_1}{\lambda_1 - \lambda_2} N_{1_0} \nu_1 e^{-\lambda_1 t} \ , \tag{7}$$

where N_{1_0} and N_{2_0} are the numbers of nuclei produced as the "cooling" starts (i.e., the irradiation stops).

The number of nuclei produced as the irradiation stops corresponds to their number as the "cooling" starts. In this case the following condition is satisfied for K irradiation pulses:

$$N_{1_0} = N_1\left[(K-1)T+\tau\right] \ , \ N_{2_0} = N_2\left[(K-1)T+\tau\right] \ . \tag{8}$$

Instead of the numbers of nuclei in experimental samples, i.e., the nuclear concentration, the actual experiment measures the counting rates in the total absorption peaks at γ-line energies E_1 and E_2, i.e., the intensities in the peaks that are related to the concentrations $N_1(t)$ and $N_2(t)$ as

$$S_1(t) = N_1(t)\lambda_1 \eta_1 \varepsilon_1 \ , \ S_2(t) = N_2(t)\lambda_2 \eta_2 \varepsilon_2 \ , \tag{9}$$

where η_1 and η_2 are the yields of the γ-lines and ε_1 and ε_2 are the spectrometric effectiveness at γ-line energies E_1 and E_2. Applying, then the condition (8) to $S_1(t)$ and $S_2(t)$), we get

$$S_1(t) = A_0 e^{-\lambda_1 t} , \tag{10}$$
$$S_2(t) = A_1 e^{-\lambda_1 t} + A_2 e^{-\lambda_2 t} , \tag{11}$$

where

$$A_0 = N_T \Phi \sigma_1 \eta_1 \varepsilon_1 F_1 , \tag{12}$$
$$A_1 = N_T \Phi \sigma_1 \eta_2 \varepsilon_2 \frac{\lambda_2}{\lambda_2 - \lambda_1} \nu_1 F_1 , \tag{13}$$
$$A_2 = N_T \Phi \eta_2 \varepsilon_2 \left(\sigma_2 - \sigma_1 \nu_1 \frac{\lambda_1}{\lambda_2 - \lambda_1} \right) F_2 . \tag{14}$$

The coefficients A_0, A_1 and A_2 that carry information on the cross sections σ_1 and σ_2 are determined by least squares-fitting the experimental points S_{1i} and S_{2i} through the respective functions

$$g(t) = A_0 e^{-\lambda_1 t} , \tag{15}$$
$$f(t) = A_1 e^{-\lambda_1 t} + A_2 e^{-\lambda_2 t} . \tag{16}$$

One constructs the quadratic functionals R_1 and R_2

$$R_1 = \sum_{i=1}^{L_1} \left(S_{1i} - A_0 e^{-\lambda_1 t_i} \right)^2 / \Delta S_{1i}^2 , \tag{17}$$
$$R_2 = \sum_{i=1}^{L_2} \left(S_{2i} - A_1 e^{-\lambda_1 t_i} - A_2 e^{-\lambda_2 t_i} \right)^2 / \Delta S_{1i}^2 , \tag{18}$$

where S_{1i} and S_{2i} are the counting rates measured in the total absorption peaks of γ-quanta of the first and second nuclide at moment t_i, ΔS_{1i} and ΔS_{2i} are the absolute errors in the above counting rates and t_i is the time span from the irradiation end to the middle of the i-th measurement interval. If L_1 and L_2 are the numbers of experimental points for the first and second nuclide, respectively, then using the condition of minimizing the functionals, we get the following expressions to find the parameters A_0, A_1, A_2 and their errors:

$$A_0 = \frac{\sum_{i=1}^{L_1} \left(S_{1i} e^{-\lambda_i t_i} / \Delta S_{1i}^2 \right)}{\sum_{i=1}^{L_1} \left(e^{-2\lambda_i t_i} / \Delta S_{1i}^2 \right)} , \tag{19}$$

$$\Delta A_0 = \left(\sum_{i=1}^{L_1} \frac{e^{-2\lambda_i t_i}}{\Delta S_{1i}^2} \right)^{-1/2} , \tag{20}$$

$$\overrightarrow{A} = M^{-1}\overrightarrow{Z} \ , \tag{21}$$

$$\Delta A_i = \sqrt{(M^{-1})_{ii}} \ , \qquad (i = 1, 2) \ , \tag{22}$$

where

$$\overrightarrow{A} = \{A_1, A_2\} \, , \qquad \overrightarrow{Z} = \begin{Bmatrix} Z_1 \\ Z_2 \end{Bmatrix} \ .$$

The matrix M and the vector of the right-hand side $\overrightarrow{Z}$ of the initial set of linear equations are

$$M_{ij} = \sum_{k=1}^{L_2} \left(e^{-(\lambda_i + \lambda_j)t_k} / \Delta S_{2k}^2 \right) \ , \tag{23}$$

$$Z_i = \sum_{k=1}^{L_2} \left(S_{2k} e^{-\lambda_i t_k} / \Delta S_{2k}^2 \right) \ , \qquad i, j = 1, 2 \ . \tag{24}$$

Calculating the cross sections necessitates determination of the proton flux Φ. With that purpose, an experimental sample was irradiated together with the Al monitor sample for which we have, by analogy with expressions (3), (10) and (12)

$$S_{Na}(t) = N_{Al} \Phi \sigma_{st} F_{Na} \eta_{Na} \varepsilon_{Na} e^{-\lambda_{Na} t} = B e^{-\lambda_{Na} t} \ , \tag{25}$$

where σ_{st} is $^{27}Al(p,x)^{24}Na$ monitor reaction cross section. The parameter B is also determined by least squares fitting the experimental points through a dependence of the form (15) using formulas (19) and (20). The number of ^{24}Na nuclei produced in the monitor will, then, be

$$N_{Na} = \frac{B}{\eta_{Na} \varepsilon_{Na} \lambda_{Na}} = N_{Al} \Phi \sigma_{st} \frac{F_{Na}}{\lambda_{Na}} \ ,$$

which permits the proton flux Φ to be presented as

$$\Phi = \frac{N_{Na} \lambda_{Na}}{N_{Al} \sigma_{st} F_{Na}} \ . \tag{26}$$

The expressions (12), (19), and (26) can be used to calculate the cumulative yield of the first nuclide (or its independent yield in case its precursors are absent):

$$\sigma_1^{cum} = \frac{A_0}{\eta_1 \varepsilon_1 F_1 N_{Na}} \frac{N_{Al}}{N_T} \frac{F_{Na}}{\lambda_{Na}} \sigma_{st} \ . \tag{27}$$

At the same time, the formulas (13), (14), (21) and (26) can be used to obtain expressions for calculating the cumulative yield of the first nuclide, as well as the independent and cumulative yields of the second nuclide:

$$\sigma_1^{cum} = \frac{A_1}{\nu_1 \eta_2 \varepsilon_2 F_1 N_{Na}} \frac{N_{Al}}{N_T} \frac{\lambda_2 - \lambda_1}{\lambda_2} \frac{F_{Na}}{\lambda_{Na}} \sigma_{st} \ , \tag{28}$$

$$\sigma_2^{ind} = \left(\frac{A_2}{F_2} + \frac{A_1}{F_1} \frac{\lambda_1}{\lambda_2} \right) \frac{1}{\eta_2 \varepsilon_2 N_{Na}} \frac{N_{Al}}{N_T} \frac{F_{Na}}{\lambda_{Na}} \sigma_{st} \ , \tag{29}$$

$$\sigma_2^{cum} = \sigma_2^{ind} + \nu_1 \sigma_1^{cum} = \left(\frac{A_1}{F_1} + \frac{A_2}{F_2} \right) \frac{1}{\eta_2 \varepsilon_2 N_{Na}} \frac{N_{Al}}{N_T} \frac{F_{Na}}{\lambda_{Na}} \sigma_{st} \ . \tag{30}$$

Obviously, the yields calculated by formulas (27) and (28) must be the same. However, the yield obtained by formula (27) is usually included in the final results because the calculation accuracy of (27) is higher.

3. Monitor reactions

As noted above, the ^{27}Al(p,x)^{24}Na reaction was used as a monitor. The ^{27}Al(p,x)^{24}Na cross section was calculated from the approximation function

$$\sigma = \sum_{i=0}^{k} a_i E^i \tag{31}$$

recommended by V.G. Khlopin Radium Institute with the coefficients tabulated in Table 1 [9].

It should be noted that Cumming [10] was the first (in 1963) who had obtained and recommended to use the values of the ^{27}Al(p,x)^{24}Na reaction excitation function. At present, however, the use of this reaction to monitor a proton flux is regarded as incorrect because the (n,α) reaction may also contribute to the yield of ^{24}Na, thus overestimating the proton flux density Φ. Therefore, the ^{27}Al(p,x)^{22}Na monitor has been preferred recently. The situation can be seen clearly in Fig. 1 showing the excitation functions of the two reactions evaluated independently at the V.G. Khlopin Radium Institute and used at ZSR (Germany) [11]. A comparison of these two plots corroborates the advantage of using the ^{27}Al(p,x)^{22}Na reaction as a monitor. At the same time, this monitor does not seem to be very attractive for us because we have to measure the short-lived (p,x) reaction products, which is particularly urgent in studying medium and heavy nuclei with reaction products form complicated decay chains. This condition restricts the irradiation times of the experimental samples since only long-lived nuclides are accumulated due to larger amont of irradiation times and hence the loading parameters of the spectometer are becoming worse. For the minor accumulation of ^{22}Na resultant from the selected short irradiation times to be measured within a high accuracy, we have to use low-background spectrometers, thus making the research much more expensive.

One can see from Fig. 1(A) that the data used at ZSR are above the V.G.Khlopin Radium Institute recommended curve by $\sim$ 10% at 100-200 MeV, by $\sim$ 5% at 600-1600 MeV and by $\sim$ 12.5% at 1600-2600 MeV. Since the accuracy of the two data groups is 10%, they can be regarded as coincident to within errors. Therefore, the possible neutron background becomes very important because its occurrence during irradiation of experimental samples would additionally increase the systematic differences among the eventual values of yields obtained by different researchers with different monitor reactions.

4. Irradiation of Experimental Samples

The yields of residual product nuclei from 1500 MeV proton irradiation were determined by exposing the experimental samples to the beam extracted by slow extraction system from the ITEP U-10 synchrotron. The extraction is schematically presented in Fig. 2. The extracted beam has the form of an ellipse with $\sim$ 25x15 mm axes, the beam intensity is $\sim 2 \cdot 10^{11}$ proton/pulse, the pulse repetition rate $\sim$ 16 min^{-1}, duration of a single pulse $\sim$ 0.5 s.

The yields of residual product nuclei from 130 MeV proton irradiation were determined by exposing the experimental samples to the proton beam used for medical purposes. The extraction is schematically presented in Fig. 3. The beam was formed by a set of collimators. The beam at the outlet of the last collimator is of circular form of ~ 15 mm diameter, $\sim 5 \cdot 10^9$ proton/pulse intensity, ~ 16 min^{-1} pulse repetition rate, and ~ 100 ns single pulse duration.

Use was made of experimental samples of metallic Bi prepared by pressing metallic powder. Before the exposure, the experimental samples were weighed with Sartorius BP-61 analytical scales and were then "soldered" together with the monitor samples and interlayers into polyethylene envelopes.

In each of the irradiation runs, a monitor-Al interlayer-experimental sample sandwich stack was placed normally to the proton beam of the respective energy. The diameters of experimental sample, interlayer and monitor were strictly the same (10.5 mm). The exposure time of a single sample was ∼15-30 min. The 1500 MeV and 130 MeV proton fluences were $\sim 2.4 \cdot 10^{13}$ and $\sim 1.5 \cdot 10^{11}$, respectively.

After the exposure, the experimental samples and the monitors were replaced into sealed polyethylene envelopes to prevent the gaseous reaction products from being lost.

The irradiation envelopes were used to check the loss of the reaction products which may escape from the irradiated experimental samples by analyzing the composition of the samples. This check demonstrated the complete absence of loss.

5. Estimation of the neutron background

In the present work, the possible neutron background in exposing experimental samples to proton beams was estimated by the SSNTD techniques used to find the parameters of medical proton beams [12]. With SSNTDs, we measured the secondary radiation background composed of neutrons and protons. In the experiment, we used the ^{209}Bi,^{238}U and ^{237}Np targets of different fission thresholds and the glass plate detectors with collimator grids. The detectors and the targets were placed near the irradiated samples at different distances from the proton beam. In calibration, the detectors and the targets were irradiated by a proton beam for a short time. Fig. 4 shows the relative distributions of the track numbers from the fission fragments recorded with the SSNTDs near the extracted 1500 MeV and 130 MeV proton beams.

The results displayed in Fig. 4 show that the secondary background is nearly isotropic and that the total number of fission fragments due to the secondary radiation near the two beams is as small as a few hundredths of one per cent of the number of the recorded fission fragments in the proton beams proper. This indicates that such a background cannot introduce any substantial distortions to the proton flux density found using the ^{27}Al(p,x)^{24}Na reaction excitation function. Surely, this is valid only if the data selected to plot the recommended dependence do not comprise the neutron background error.

6. Measurement and processing of γ-ray spectra

The measurement facility is a spectrometric circuit comprising a GC-2518 Ge detector, a 1510 module (ADC, amplifier, high-voltage supply), and a S-100 base that as an integral part of an IBM PC emulates a multichannel analyzer. The ^{60}Co 1332 keV γ-line energy

resolution of the facility is 1.8. keV. Fig. 5 presents the measured γ-spectra of the (p, x) reaction products.

The γ-spectra measured were processed by the PC IBM-realized ASPRO code [13]. The spectra thus processed were combined to form an input file for the SIGMA code. The code plots the intensity of a selected γ-line versus time and, using its energy and simulated half-life, identifies the produced nuclides by the GDISP database and simulates their cross sections by formulas (27-30) [14].

The measured γ-spectra are of high intensity, especially during the early decay period. Therefore, any possible detection losses under high loads of the spectrometer must be checked out carefully. To avoid the associated systematic errors, the spectrometer was checked out by the method of two sources. Fig. 6 shows the variations in the peak area and resolution versus the spectrometer load.

Conforming to these results, the ultimate load of the spectrometer was limited so as not to exceed 5% in all of the measurements. To remain within that limitation, we started monitoring the experimental samples at ∼500 mm height and, as the load decreased, descended down to the ultimate height of 40 mm. The γ-spectra measured were correlated to each other by introducing the height factors determined by the function $R(x) = a/(b + x)^2$ with constants calculated by approximating the experimental points. Fig. 7 shows a plot of this function.

The independent and cumulative yields of the reaction products in formulas (27-30) were calculated using the relative spectrometric effectiveness. Fig. 5 shows the analytical dependence of the spectrometric effectiveness in the 36.5-2650.0 keV range. The techniques of determining the effectiveness are described in [15].

In addition, we have used in our measurements also a low-background spectrometer with ∼50 and ∼100 decay/hour ultimate sensitivities of its Ge-Li detector at 1500 keV and 200-300 keV, respectively. This spectrometer was designed for measuring the magnetic moment of the neutrino and has a counterpart described in [16]. This spectrometer was used to measure γ-spectra of experimental samples 1.5 years after the samples were irradiated. Cross sections of long-lived nuclear reaction products were obtained by identifying and analyzing these γ-spectra.

The corrections for γ-absorption in the substances of experimental or monitor samples were calculated using a expression published in [17]. The values of the total linear attenuation factor μ were taken from [18].

7. Experimental Results

Tables 2 through 5 present the results of measuring the independent and cumulative yields of the ground and metastable states of the ^{209}Bi nuclear reaction products at proton energies of 1500 MeV and 130 MeV. Table 2 presents the experimental cumulative yields of the ground states of the reaction products, Table 3, the experimental and simulated independent yields of the ground states of the reaction products, Table 4, the experimental and simulated independent and cumulative yields of the metastable states of the reaction products and Table 5, the total experimental yields of the ground and metastable states together with the simulated yields of the ground states of the reaction products.

The ^{27}Al(p,x)^{24}Na cross sections were calculated according to (31) and are taken to be 9.9±1.0 mb and 9.6±1.0 mb at 1500 MeV and 130 MeV proton energies, respectively.

It should be noted that the experimental values have been renormalized to the quantum yields in the PCNUDAT nuclear database [19] and Table of Isotopes (8th Edition) [20]. The renormalization has become necessary because the tabulated experimental yields of reaction products were obtained for many of the nuclides by averaging over several γ-lines. When varying the recommended γ-quantum yield data, therefore, their separate values have to be renormalized and averaged again. The complete information cannot be published in practice because it is too voluminous. The reaction yields obtained using the low-background spectrometer are labelled (*).

Fig. 8 shows some of the most characteristic plots of the time dependences of the ^{209}Bi(p,x) reaction product decays.

In the case of ^{209}Bi irradiated by 1500 MeV protons, Fig. 8(A) shows the time dependencies of two independent ^{179}Re and ^{198}Pb decays at $E_\gamma \sim 290.0$ keV and of the independent ^{95}Tc decay together with the decay chain ^{95}Zr$\rightarrow^{95}$Nb of parent nuclides at $E\gamma \sim 765.8$ keV. In the case of ^{209}Bi irradiated by 130 MeV protons, Fig. 8(B) shows the time dependencies of the independent ^{205}Po decay at $E\gamma = 872.4$ keV, of the decay chain ^{201}Bi$\rightarrow^{201}$Pb of parent nuclides at $E\gamma = 331.2$ keV. From Fig. 8 it can be seen that the analyzing the decay curves of the nuclear reaction products may be much more complicated compared with the simplified case described above in the section 2. This is due, first of all, to the fact that the nuclear transition energies of the reaction products may prove to be so alike that the actual unresolvable γ-lines occur in the measured γ-spectra. Given the situations like the above, the SIGMA code realizes the feasibility of separating them by the least squares method and in view of the fact that the nuclides produced are of different half-lives. One of the SIGMA subroutines separates the nuclide decays by independent decay chains, while another separates an independent nuclide decay from a chain of parent nuclides.

8. Measurement errors

Analyzing the errors in the results obtained has shown that they fall mostly within $\cong (10 \div 35)\%$. The values of the errors were calculated as follows. Since the results presented were obtained mostly by averaging several $(\sigma_i \pm \Delta\sigma_i)$ values calculated for different γ-lines, their means and their errors were calculated using formulas

$$\overline{\sigma} = \frac{\sum_i \sigma_i W_i}{\sum_i W_i}, \qquad \text{where} \qquad W_i = 1/\Delta\sigma_i^2 \ , \tag{32}$$

$$\Delta\overline{\overline{\sigma}} = \sqrt{\frac{\sum_i W_i \left(\overline{\sigma} - \sigma_i\right)^2}{(n-1)\sum_i W_i}} \ . \tag{33}$$

The total error in the values presented in Tables 2, 3, 4, 5 was calculated making allowance for the monitor error as

$$\frac{\Delta\overline{\sigma}}{\overline{\sigma}} = \sqrt{\left(\frac{\Delta\overline{\overline{\sigma}}}{\overline{\sigma}}\right)^2 + \left(\frac{\Delta\sigma_{st}}{\sigma_{st}}\right)^2} \ . \tag{34}$$

The errors in the independent and cumulative yields of the reaction products for separate γ–lines, $\Delta\sigma_i$ calculated by formulas (33) and (34) were determined using the formulas for transfer of errors.

As shown by the analysis, the uncertainties in the nuclear data on γ-yields and on monitor reaction cross sections make the major contribution to the total error.

9. Theoretical simulation of measured products

9.1. Technique of comparing experimental and simulated results

The simulation results should be compared with the experimental data making allowance for the fact that any of the computer simulation codes can only simulate the independent yields of nuclear reaction products, whereas most of the experimental data are the cumulative yields. So, any correct comparison must involve a procedure for calculating a simulated cumulative yield on the basis of the simulated independent yields of the respective precursors.

If the production chain of n nuclides is presented as

$$\begin{array}{ccccccc} \downarrow \sigma_1 & & \downarrow \sigma_2 & & \dots & & \downarrow \sigma_n \\ \boxed{1} & \overset{\nu_1,\lambda_1}{\rightarrow} & \boxed{2} & \overset{\nu_2,\lambda_2}{\rightarrow} & \dots & \overset{\nu_{n-1},\lambda_{n-1}}{\rightarrow} & \boxed{\mathrm{n}} \end{array} ,$$

the cumulative yield of the last (n-th) nuclide can be calculated as

$$\sigma_n^{cum} = \sum_{i=1}^{n} \sigma_i^{ind} l_i \ , \tag{35}$$

where l_i is the fraction of decays of nuclide i that go to nuclide n, which is defined using the branching factors ν_j as

$$\begin{cases} l_i = \prod\limits_{j=1}^{n-1} \nu_j, & i < n \ , \\ \\ l_i = 1, & i = n \ . \end{cases}$$

The above representation ensures from the conceptual physical treatment of the independent and cumulative yields and is corroborated by the form of formulas (28-30). The values of the nuclear chain branching factors have been taken from [21] . Unfortunately, lack of any fresher systematized data has made us use the somewhat obsolete values of the factors. The data are very difficult to extract from the renewed databases, and the extraction procedure falls outside the scope of the present research program. Surely, use of any newer data may have affected the accuracy of the simulated cumulative yields of the reaction products. At the same time, identical values are very important to use when comparing the experimental data and the simulation results obtained by different codes.

To get a correct comparison among the data simulated by different codes, the simulation results are to be renormalized to unified the cross section of the proton-nucleus interaction, using available experimental data values or phenomenological formulas. Here we used Letaw's formulae described in [22] to obtain the unified cross section to be 1663 mbarn at 130 MeV and 1873 mbarn at 1500 MeV.

If a comparison event with simulation differing from experiment by not more than a factor of 2 is assumed here to be the coincidence criterion, then the predictive power of the codes can be presented via a ratio of the number of coincidences to the total number

of comparison events. Another parameter proposed in [8] to present code accuracies is the mean deviation of simulation results from experimental data:

$$\langle H \rangle = 10^{\sqrt{\langle \left(lg \left(\frac{\sigma_{cal}}{\sigma_{exp}} \right) \right)^2 \rangle}} , \tag{36}$$

where $\langle\ \rangle$ designates averaging over all of the comparison events.

9.2. Computer simulation codes

The products of ^{209}Bi(p,x)-reaction were simulated by seven different codes, namely,

- the CEM95 Cascade-Exciton Model code [23, 24],
- the CASCADE cascade – evaporation – fission transport code [25],
- the INUCL cascade – preequilibrium – evaporation – fission code [26],
- the HETC cascade – evaporation transport code [27],
- the LAHET cascade – evaporation – fission transport code [28],
- the GNASH code based on the Hauser-Feshbach and preequilibrium approach [29],
- the ALICE code with HMS precompound approach [30].

A detailed description of the models used by these codes may be found in Refs. [23]-[30] and references given therein; therefore, only their basic assumptions will be outlined below.

CEM95 uses the Monte Carlo method to simulate hadron-nucleus interactions in the framework of an extended version [24] of the Cascade-Excitom Model (CEM) of nuclear reactions [23]. The CEM assumes that the reactions occur in three stages. The first stage is the intranuclear cascade in which primary and secondary particles can be rescattered several times prior to absorption by, or escape from the nucleus. The excited residual nucleus remaining after the emission of the cascade particles determines the particle-hole configuration that is the starting point for the second, preequilibrium stage of the reaction. The subsequent relaxation of the nuclear excitation is treated in terms of the exciton model of preequilibrium decay which includes the description of the equilibrium evaporative third stage of the reaction.

The cascade stage of the interaction is described by the standard version of the Dubna intranuclear cascade model (INC) [31]. All the cascade calculations are carried out in a three-dimensional geometry. The nuclear matter density $\rho(r)$ is described by a Fermi distribution with two parameters taken from the analysis of electron-nucleus scattering, namely

$$\rho(r) = \rho_p(r) + \rho_n(r) = \rho_0\{1 + exp[(r-c)/a]\} ,$$

where $c = 1.07A^{1/3}$ fm, A is the mass number of the target, and $a = 0.545$ fm. For simplicity, the target nucleus is divided by concentric spheres into seven zones in which

the nuclear density is considered to be constant. The energy spectrum of the target nucleons is estimated in the perfect Fermi gas approximation with the local Fermi energy $T_F(r) = \hbar^2[3\pi^2\rho(r)]^{2/3}/(2m_N)$, where m_N is the nucleon mass. The influence of intranuclear nucleons on the incoming projectile is taken into account by adding to its laboratory kinetic energy an effective real potential V, as well as by considering the Pauli principle which forbids a number of intranuclear collisions and effectively increases the mean free path of cascade particles inside the target. For incident nucleons $V \equiv V_N(r) = T_F(r) + \epsilon$, where $T_F(r)$ is the corresponding Fermi energy and ϵ is the mean binding energy of the nucleons ($\epsilon \simeq 7$ MeV [31]). For pions, in the Dubna INC one usually uses [31] a square-well nuclear potential with the depth $V_\pi \simeq 25$ MeV, independently of the nucleus and pion energy. The interaction of the incident particle with the nucleus is approximated as a series of successive quasifree collisions of the fast cascade particles (N or π) with intranuclear nucleons:

$$\begin{aligned} NN \to NN, \qquad NN \to \pi NN, \qquad NN \to \pi_1, \cdots, \pi_i NN \ , \\ \pi N \to \pi N, \qquad \pi N \to \pi_1, \cdots, \pi_i N \qquad (i \geq 2) \ . \end{aligned} \tag{37}$$

To describe these elementary collisions, one uses experimental cross sections for the free NN and πN interactions, simulating angular and momentum distributions of secondary particles using special polynomial expressions with energy-dependent coefficients [31] and one takes into account the Pauli principle. Besides the elementary processes (37), the Dubna INC also takes into account pion absorption on nucleon pairs

$$\pi NN \to NN. \tag{38}$$

The momenta of two nucleons participating in the absorption are chosen randomly from the Fermi distribution, and the pion energy is distributed equally between these nucleons in the center-of-mass system of the pion and nucleons participating in the absorption. The direction of motion of the resultant nucleons in this system is taken as isotropically distributed in space. The effective cross section for absorption is related (but not equal) to the experimental cross sections for pion absorption by deuterons.

The standard version of the Dubna INC is described in detail in the monograph [31] and more briefly, in the review [32] and in the recent book by Iljinov, Kazarnovsky, and Paryev [33]. A detailed comparison of the Dubna INC with the well known Bertini INC developed at Oak Ridge National Laboratory [34] and with the popular version developed at Brookhaven National Laboratory and Columbia University by Chen et al. [35] is made in Ref. [36].

An important point of the CEM is the condition for transition from the intranuclear cascade stage to preequilibrium processes. In a conventional cascade-evaporation model, cascade nucleons are traced down to some minimal energy, the cut-off energy T_{cut} being about 7–10 MeV, below which particles are considered to be absorbed by the nucleus. In the CEM [23], it was proposed to relate the condition for a cascade particle to be captured by the nucleus to the similarity of the imaginary part of the optical potential calculated in the cascade model $W_{opt.mod.}(r)$ to its experimental value $W_{opt.exp.}(r)$ obtained from analysis of data on particle-nucleus elastic scattering. The agreement between $W_{opt.mod.}$ and $W_{opt.exp.}$ is assumed to occur when the proximity parameter

$$\mathcal{P} = \mid (W_{opt.mod.} - W_{opt.exp.})/W_{opt.exp.} \mid$$

becomes small enough. In CEM95, a fixed value $\mathcal{P} = 0.3$ extracted from the analysis of experimental proton- and pion-nucleus data at low and intermediate energies is used.

The subsequent interaction stages (preequilibrium and equilibrium) of nuclear reactions are considered in the CEM in the framework of an extension of the Modified Exciton Model (MEM) [37, 38]. At the preequilibrium stage of a reaction the CEM takes into account all possible nuclear transitions changing the number of excitons n with $\Delta n = +2, -2$, and 0, as well as all possible multiple subsequent emissions of n, p, d, t, ^{3}He, and ^{4}He. The corresponding system of master equations describing the behavior of a nucleus at the preequilibrium stage is solved by the Monte Carlo technique [38].

Let us note here that in the CEM the initial configuration for the preequilibrium decay (number of excited particles and holes, i.e. excitons $n_0 = p_0 + h_0$, excitation energy E_0^*, linear momentum $\boldsymbol{P}_0$ and angular momentum $\boldsymbol{L}_0$ of the nucleus) differs significantly from that usually postulated in exciton models.

To be able to analyze reactions with heavy targets and to describe accurately excitation functions over a wider range of incident particle energy, the CEM has been extended recently [24]. The extended version incorporates the competition between evaporation and fission of compound nuclei, takes into account pairing energies, considers the angular momentum of preequilibrium and evaporated particles and the rotational energy of excited nuclei, and can use more realistic nuclear level densities (with Z, N, and E^* dependences of the level density parameter).

The extended version of the CEM realized in the code CEM95 is described in details in Ref. [24]. A detailed analysis with CEM95 of more than 600 excitation functions for proton induced reactions on 19 targets ranging from ^{12}C to ^{197}Au, for incident energies ranging from 10 MeV to 5 GeV and a comparison to available data, to calculations using approximately two dozen other models, and to predictions of several phenomenological systematics is presented in the next paper by Mashnik et al. [39] in this issue. A comparison of many excitation functions calculated with CEM95 with predictions of several other codes may be found in the recent NEA/OECD document [8]. In present work, all calculations with CEM95 were performed using for the macroscopic fission barriers the Yukawa-plus-exponential modified LDM of Krappe, Nix and Sierk [40], and Cameron's shell and pairing corrections [41] for the ground state and Barashenkov et al. [42] corrections for the saddle-point masses for microscopic fission barriers; the third Iljinov's et al. systematics for the level density parameters [43], with shell corrections by Cameron et al. [44], without taking into account the dependence of fission barriers on angular momenta, with the dependence of fission barriers on excitation energy proposed in Ref. [45], and with a fixed value of 1.082 for the ratio a_f/a_n for both incident energies. All values of other CEM parametrs are fixed and are the same as in Refs. [23, 24].

The codes included into the CASCADE complex [25] have been developed and employed for many years in the Laboratory of Computing Technique and Automation of JINR, Dubna to describe interactions of hadron and nuclei with nuclei and with gaseous and condensed matter.

Calculation of intranuclear cascades is performed in diffuse nucleon clouds, the space distribution of which is defined from experiments on electron scattering. The model takes into consideration the competition of evaporation and fission processes in excited nuclei remaining after the completion of the cascade and preequilibrium (described, according to [38]) processes. Inelastic interaction of the nuclei appears as a superposition of two-

particle nucleon-nucleon and pion-nucleon collisions which can occur both in the nuclear overlap region and inside each nucleus separately (see the second paper in Ref. [25]). Interaction of cascade particles with intranuclear nucleons occur also in the case when the interacting nuclei are already separated and continues till all of the cascade particles are either absorbed by the nuclei or escape the nuclei. Mutual interactions of the cascade particles are neglected. The number of nucleons in the clouds (Fermi particles) is equal to mass numbers of striking nuclei in the beginning of the process and gradually decreases due to knocking out of the nucleons by the growing shower of cascading particles (the so-called "trawling" effect). Therefore, the coordinates of all nucleons are simulated in the beginning of the collision and are redefined during the calculation procedure depending on the cascade development. At a starting point t, corresponding to a moment when the colliding nuclei come into contact, all particle collisions permitted by kinematics and the Pauli principle are simulated. Only one which takes place earlier than the others is chosen ($dt = min\{t_i\}$); after that the positions of the interacting nucleons and all cascading particles (nucleons and produced pions) are shifted to the new points corresponding to the moment of time $t + dt$. The calculation procedure is further repeated until all the cascade particles in the colliding nuclei are exhausted (see details in the third paper of Ref. [25]). Decay of the excited nuclei is calculated basing on the evaporation model as described in [31] with a fixed level density parameter which is taken to be a=A/10 [MeV^{-1}]. In order to consider the internuclear cascades in material samples the codes are supplied with simulation of the particle transport including energy losses on ionization, definition of the interaction point considering the boundaries of the media with different chemical composition. Neutron transport is calculated basing on the 26-group system of neutron cross-sections.

The cascade – preequilibrium – evaporation – fission code INUCL was developed during several years at ITEP, Moscow by Stepanov with co-authors [26]. The cascade stage of INUCL was inspired by the standard Dubna INC [31] but differs from it in several points, as: use of new, more complete than in [31] experimental data for cross sections of elementary NN and πN processes (37), the range of incident particle energies was extended in INUCL up to 15 GeV (in the standard Dubna INC, it is only up to about 5 GeV), use of a different radial distribution of nuclear pairs absorbing pions inside a nucleus (38), taking into account the local reduction of nuclear density ("trawling" effect) at energies above several GeV and several other details (see the first paper of Ref. [26]).

The preequilibrium stage of INUCL was inspired by the MEM [37, 38] and CEM [23] but differs from the Dubna version by using another approach for the squared matrix elements of the transition rates and by neglecting emission of complex particles and not taking into account the forward peaked angular distributions of preequilibrium nucleons (see details in the second paper of Ref. [26]).

The evaporation model in INUCL was also inspired by the Dubna version [31, 38], except the use of other level density parameters and, at low excitation energies (below the separation energy of nucleons or complex particles), calculation of emission of low-energy gammas (see details in the second paper of Ref. [26]).

The most interesting point of INUCL is incorporation at the evaporation stage of reactions of a new, "home-grown" thermodynamical model of high energy fission (see the third and fourth papers in Ref. [26]). From a physical point of view, the thermodynamical model of fission is statistical by nature, but provides A-, Z- and energy-distributions of

fission fragments quite different from the well known Fong's statistical model of nuclear fission [46], uses a own systematics for the ratio of level density parameters a_f/a_n, and seems to describe experimental data better (see details in the third and fourth papers of Ref. [26]).

The popular transport cascade – evaporation code HETC [27] was developed at Oak Ridge National Laboratory. HETC is basically an extension of the code NMTC [47] to allow particle transport up to several hundred GeV [27]. For nonelastic collisions at energies below $\sim$ 3 GeV, HETC uses Bertini INC model [34] at the cascade stages of reactions and Guthrie's evaporation program [48] to determine the energy and direction of emitted cascade nucleons and pions and evaporated n, p, d, t, ^{3}He and α-particles, and the mass, charge, and recoil energy of the residual nucleus.

As we mentioned above, a detailed comparison of the Bertini INC [34] with the Dubna INC [31] and with Chen's et al. INC [35] may be found in Ref. [36]. We use on our work the standard version of HETC [27], well known and widely used in many laboratories, therefore we do not consider necessary to repeat here its detailed description.

LAHET is a Monte Carlo code for the transport and interaction of nucleons, pions muons, light ions, and antinucleons in complex geometry [28]; it may also be used without particle transport to generate particle production cross sections. LAHET is the result of a major effort at Los Alamos National Laboratory to develop a code system based on the LANL version of the HETC Monte Carlo code for the transport of nucleons, pions and muons, which was originally developed at Oak Ridge National Laboratory [27, 49]. Due to many new features added at LANL, the code has been renamed LAHET, and the system of codes based on LAHET designated as the LAHET Code System (LCS) [28].

LAHET can use Bertini INC [34] (from HETC) to describe nucleon-nucleus interactions below 3.5 GeV, and a scaling law approximation to continue the interaction energy to arbitrary high energies, although a reasonable upper limit is about 10 GeV.

As an alternative to the Bertini INC, LAHET contains the INC routines from ISABEL code. The ISABEL INC model is an extension by Yariv and Fraenkel [50] of the VEGAS code [35] mentioned above. ISABEL has the capability of treating nucleus-nucleus interactions as well as particle-nucleus interactions. In the present work, we use both Bertini INC and ISABEL versions of the INC to perform calculations with LAHET.

Let us mention here two more points between the interesting features of LAHET (see details in [28]). First, LAHET allows one to calculate preequilibrium processes as an intermediate stage between the intranuclear cascade and evaporation/fission in the framework of a multistage multistep preequilibrium exciton model ("MPM") [51]. As initially suggested and used in the MEM [37, 38], the MPM uses the Monte Carlo method to solve the system of master equations describing the process of equilibration of excited residual nucleus remaining after the cascade stage of a reaction. Nevertheless, there are several important differences between MPM and MEM. First, the master equations of the MPM is simplified as compared to the one of MEM: MPM takes into account only nuclear transitions with $\Delta n = +2$, i.e., only in the direction of equilibration, while the MEM considers all possible transitions $\Delta n = +2, = -2$, and $=0$, accounting for all possible positions of the particle-hole pairs with respect to the Fermi level (transitions with $\Delta n = 0$). Then, the master equations of the MPM does not take into account the angular distributions of preequilibrium particles (it should be noted, that as an option,

the MPM and correspondingly the code LAHET, allow to calculate angular distributions of preequilibrium particles by using the phenomenological parametrization of Kalbach (see [51])), while the MEM does this and the version of the MEM used in CEM95 takes into account the conservation of momentum and angular momentum of the nuclear system at both preequilibrium and evaporation stages of a reaction. Then, the Monte Carlo algorithms used in the MPM amd MEM for solving the corresponding master equations also differ. There are several other differences between the MPM and MEM as using of different approximations for the inverse cross sections and Coulumb barriers, for the level density parametrs and for the matrix elements of nuclear transitions, etc. (see details in [37, 38, 51]). Note, that the interface between the intranuclear cascade model and the MPM and the interface between MPM and the evaporation model [53] used in LAHET and the ones used in CEM95 are also different.

Let us note also that LAHET includes as user options two models for fission induced by high energy iteractions: the ORNL model [52], and the Rutherford Appelton Laboratory (RAL) model by Atchinson [54]; the fission models are employed with the evaporation model. The RAL model allows fission for $Z \geq 71$, and is the default fission model in LAHET. The RAL model really is two models, for actinide and for subactinide fission. A detailed description of the models incorporated in the LCS may by found in Ref. [28] and is available on the World Wide Web in several documents (see [28]).

The GNASH code [29] applies the Hauser-Feshbach theory to calculate the decay of compound nuclei in an open-ended sequence of decay chains, conserving angular momentum and parity at all stages of the reaction. Prior to equilibrium decay, the preequilibrium emission of fast particles is accounted for using the exciton model, for up to two preequilibrium ejectiles prior to equilibration. The exciton model also includes angular momentum considerations to determine the spin distributions of residual nuclei after preequilibrium emission [55]. Transmission coefficients are calculated from the optical model, and the continuum (statistical) level density formalism of Ignatyuk et al. is matched onto experimental low-lying discrete levels. In this way, radionuclide production can be calculated to both the ground state, and isomeric states.

The ALICE code calculates equilibrium decay with the Weisskopf-Ewing theory, and preequilibrium emission is determined using the new Hybrid Monte Carlo Simulation (HMS) model [30]. This model follows successive interactions of excited nucleons creating three quasi-particle excitations during the equilibration process. Importantly, the theory is able to account for any number of multiple preequilibrium processes in a natural way – a major advantage over some other preequilibrium models which only consider a maximum of two preequilibrium ejectiles. The model has been applied successfully at energies up to 400 MeV for the calculation of excitation functions [30, 56].

Since most of simulation codes (except for GNASH) cannot simulate the metastable states of product nuclei, the respective nuclide chains used to simulate the cumulative yields of the product nuclei were taken to be simplified.

The results obtained by the codes are displayed in two sets of figures, first, in Figs. 9 and 10, which show the product mass distribution for $E_p = 130$ MeV and 1500 MeV, respectively, and, second, in Figs. 11 and 12, which present the simulation-to-experiment ratios versus relative mass difference between an initial target nucleus and a particular

product nucleus for E_p = 130 MeV and 1500 MeV, respectively. Together with the simulated results, Figs. 9 and 10 show experimental data obtained by summing the yields with respect to all the available isobar decay chains making allowance for their cumulating effect.

The E_p = 1500 MeV experimental results shown in Fig. 10 are a visual demonstration of the different production channels, namely, due to spallation reactions for masses ranging from ∼125 to 210 and due to fission reactions for masses ranging from ∼30 to ∼140. The range of masses from ∼125 to ∼140 is most probably transient, where the reaction products can be generated by both channels. The E_p = 130 MeV experimental results shown on Fig. 9 demonstrate only the production channel due to spallation reactions for masses ranging from ∼190 to 207. The lack of experimental data for the fission product masses is accounted for by the poor exposure conditions of the experimental samples.

Table 3 presents the experimental and simulated independent yields of the ground states of ^{209}Bi(p,x)–reaction products at E_p = 1500 MeV and 130 MeV for some of the nuclear reaction product yields. Table 4 presents the experimental and simulated values of the independent and cumulative yields of the metastable states of ^{209}Bi(p,x)–reaction products at E_p = 1500 MeV and 130 MeV. The simulation results relate only to E_p = 130 MeV since the GNASH code is valid for simulation of proton interactions with initial energy below threshold of pion productions (∼ 0.2 GeV)

Table 5 presents the total experimental values of the ^{209}Bi(p,x)–reaction product ground and metastabe states at E_p = 1500 MeV together with the respective simulated ground states.

9.3. Comparison between experiment and simulation

Table 6 presents the information that shows the predictive power of each code for both energies, namely, coincidence statistics which include number of experimentally measured products N_{EXP}, number of simulated products that were measured N_S, number of "coincidences" between simulated and experimental values N_C and the mean deviation $\langle H \rangle$ of simulation results from experimental data

Obviously, the simulation results shown on Figs. 9 and 10 do not contradict the experimental data if the simulated values run above the experiment and repeat their general trend. The explanation is that the direct precision γ-spectrometry technique used in this work makes it possible only to identify the radioactive products of a high yield that includes a significant part of the total yield of a given mass. Unlike the cumulative yields, the independed yields makes possible to performe the direct comparison with corresponding calculated values.

As seen from Tables 3, 4 and 5 the majority of the simulated results agree well with the experimental values. However, in some cases the simulation results are underestimated significantly comparing with the experimental data, especially for short-lived products. There are a set of particular products whose simulated yields described by the majority of the used codes are below the experimental ones by several orders of magnitude.

The following conclusions concerning the scope of applicability of the simulation codes can be drawn from comparing simulation and experiment results:

- INUCL describes quite reliably spallation products with masses above A=180 and fission products with masses below A=120; the products in the intermediate mass

region A=120 to 180 are underestimated basically by a factor of 2 to 5; analysis of particular products shows that the code underestimates significantly, up to a few orders of magnitude, the short-lived products (see, e.g., the yields of ^{203}Po and ^{202}Po),

- HETC properly describes the spallation region, though, at E_p = 150 MeV, a too large underestimation for production of ^{201}Pb and, especially of ^{200}Tl was obtained; since the available version of the code does not include the fission processes, it cannot be used for predicting fission products,

- CEM95 also predicts only spallation products but does it most perfectly compared with the other codes; a new version of the CEM realized in the code CEM97 (now in progress, see [39]) is expected to be even more succesful in the spallation region and is extended to describe also production of daughter nuclides in the fission and fragmentation regions,

- CASCADE describes satisfactorily the production of most nuclides in the spallation region but overestimates some yields of nuclides in the intermediate mass region from A=178 to about 195 and strongly underpredicts production of several short-lived nuclides (see, e.g., the yields of ^{200}Tl, ^{198}Tl in the spallation region and the yield of ^{146}Eu in the intermediate region),

- LAHET predicts the yields of most measured nuclides within a factor of 2 both in the spallation and fission regions, as well as in the intermediate mass region; nevertheless, some too big discrepancies were obtained for ^{200}Tl (at E_p = 130 MeV) in the spallation region, for ^{146}Eu and ^{140}La in the intermediate region, and for ^{82}Br and ^{76}As in the fission region,

- GNASH is the only code used here capable of calculating metastable states and has predicted the yields of ^{202m}Pb and ^{197m}Pb well; it also described within a factor of 2 the production of most ground state isotopes in the spallation region, except the yields of ^{206}Bi and ^{201}Pb,

- ALICE also predicted the yields of most isotopes in the spallation region within a factor of 2, except production of ^{201}Pb, ^{200}Tl, and ^{198}Tl.

10. Conclusion

This study is the first step in our work on non-fissible targets of interest for accelerator-driven facilities. Final conclusions about the predictive properties of the codes should thus be drawn in a following paper. At the present time, we can draw only a preliminary conclusion that theoretical yields predicted by different codes differ sometimes up to two orders of magnitude. This is a strong indication that further development of all codes is necessary before they can become reliable predictive tools.

Acknowledgments

We thank N.V. Stepanov for useful theory discussions and, especially, to F.K. Chukreev (Kurchatov Institute) for his helpful comments concerning nuclear decay chains data. One of the authors (S. G. M.) is grateful to R. E. MacFarlane, D. G. Madland, P. Möller, J. R. Nix, A. J. Sierk, L. Waters and P. G. Young of LANL for many helpful discussions and support.

The work was made under the ISTC Project # 017 and was completed under the auspices of the U.S. Department of Energy by the Los Alamos National Laboratory under contract no. W-7405-ENG-36.

References

[1] F. Carminati, R. Klapisch, J.P. Revol, Ch. Roche, J.A. Rubio and C. Rubbia, CERN Report CERN/AT/93-47(ET) (1993); C. Rubbia, J.A. Rubio, S. Buono, F. Carminati, N. Fiétier, J. Galvez, C. Gelès, Y. Kadi, R. Klapisch, P. Mandrillon, J. P. Revol and C. Roche, CERN Report CERN/AT/95-44(ET) (1995).

[2] C.D. Bowman, in: Proc. Workshop on Nuclear Transmutation of Long-Lived Nuclear Power Radiowastes, Obninsk, Russia, July 1-5, 1991, p. 127; C.D. Bowman, in: Proc. Int. Conf. on Accelerator-Driven Transmutation Technologies and Applications, Las Vegas, NV, July 25-19, 1994, AIP Conf. Proceedings 346 (1994) p. 22.; F. Venneri, C.D. Bowman, M.A. Williamson, L. Ning, T.S. Bhatia, R.J. Jensen, B.E. Newnam and S.A. Wender, Los Alamos National Laboratory Report LA-UR 96-500 (1996); C.D. Bowman, in: Proc. Int. Workshop on Nucl. Methods for Transmutation of Nuclear Wastes: Problems, Perspectives, Cooperative Research, Dubna, Russia, May 29-31, 1996, eds. M.Kh. Khankhasayev, Zh.B Kurmanov and H. Plendl (World Scientific, Singapore, 1997) p. 257.

[3] T. Takizuka, H. Takada and I. Kanno, in: Proc. Workshop on Nuclear Transmutation of Long-Lived Nuclear Power Radiowastes. Obninsk, Russia, July 1-5, 1991, p. 79; T. Takizuka, T. Nishida, T. Sasa, H. Takada, S. Meigo, M. Mizumoto and K. Hasegawa, in: Proc. Int. Conf. on Evaluation of Emerging Nucl. Fuel Cycle Systems, GLOBAL '95, Versailles, France, September 11-14, 1995, p. 489.

[4] V.D. Kazaritsky, in: Proc. Second Int. Conf. on Accelerator-Driven Transmutation Technologies and Applications, Kalmar, Sweden, June 3-7, 1996 (in press).

[5] V.G. Vasil'kov, V.I. Gol'danskii, V.P. Dzhelepov and V.P. Dmitrievskii, Atomnaya Energya 29 (1970) 151 (in Russian).

[6] A.J. Koning Report ECN-C-93-005, Petten (January 1993); Report ECN-C-93-041, Petten (June 1993).

[7] R. Michel, M. Gloris, H.-J. Lange, I. Leya, M. Lpke, U. Herpers, B. Dittrich-Hannen, R. Rösel, Th. Sciekel, D. Filges, P. Dragovitsch, M. Suter, H.-J. Hoffmann, W. Wölfli, P.W. Kubik, H. Bauer and R. Wieler, Nucl. Instr. and Meth. B. 103 (1995) 183.

[8] R. Michel and P. Nagel, International Codes and Model Intercomparison for Intermediate Energy Activation Yields, NEA/OECD, Paris, 1997, NSC/DOC(97)-1; see also the Web page at: http://www.nea.fr/html/science/pt/ieay.

[9] Yu.V. Aleksandrov, V.P. Eismont, R.B. Ivanov, L.M. Krizhansky, M.A. Mikhailova, V.P. Prikhodtseva, A.V. Saulsky and S.K. Vasiliev, in: Abstracts of the Reports of the Int. Conf. on Nucl. Phys. (XLVI Meeting on Nuclear Spectrometry and Nuclear Structure), Moscow Russia, June 18-21, 1996 (St.-Petersburg, 1996) p. 223.

[10] J.B. Cumming, Annu. Rev. Nucl. Sci. 13 (1963) 261.

[11] R. Michel, R. Bodermann, H. Busemann, R. Daunke, M. Gloris, H.-J. Lange, B. Klug, A. Krins, I. Leya, M. Lpke, S. Neumann, H. Reinhardt, M. Schnatz-Büttgen, U. Herpers, Th. Sciekel, F. Sudbrock, B. Holmqvist, H. Condé, P. Malmborg, M. Suter, B. Dittrich-Hannen, P.W. Kubik, H.-A. Synal and D. Filges, Nucl. Instr. and Meth. B. 129 (1997) 153 and references theirein; see also the Web page at: http://sun1.rrzn-user.uni-hannover.de/zsr/survey.htm#url=overview.htm.

[12] M.F. Lomanov, G.G. Shimchuk and R.M. Yakovlev, Health Physics 39 (1979) 677; M.F. Lomanov, B.I. Reznik, G.G. Shimchuk and R.M. Yakovlev, Atomnaya Energiya 45 (1978) 350 (in Russian).

[13] V.V. Atrashkevich, Ya.K. Vaivade, V.P. Kolotov and V.V. Filippov, Akademicheskaya Khimiya 45 (1990) 5 (in Russian).

[14] L. Spanier and P. Ekstrom, Nuclear Physics Report LUNFD6 (NFFR-3059)/1-11, Lund, Sweden (1989).

[15] Yu.E. Titarenko, O.V. Shvedov, M.M. Igumnov, E.I. Karpikhin, V.I. Volk, A.Yu. Vakhrushin, S.V. Shepelkov, A.V. Lopatkin, S.G. Mashnik and T.A. Gabriel, submitted to Nucl. Sci. Eng.; Yu.E. Titarenko, O.V. Shvedov, M.M. Igumnov, E.I. Karpikhin, A.V. Lopatkin, V.I. Volk, A.Yu. Vakhrushin, S.V. Shepelkov, S.G. Mashnik and T.A. Gabriel, submitted to Nucl. Sci. Eng.

[16] A.A. Vasenko, Yu.N. Vereshchagin, I.V. Kirpichnikov, V.A. Kuznetsov, V.N. Prusakov, A.I. Rudnev, A.S. Starostin and A.V. Tikhomirov, Pribory i Tekhnika Experimenta 2 (1989) 56 [Instruments and Experimental Techniques 32 (1989) 312].

[17] P.F. Zweifel and A. Arbor, Nucleonics 18 (1960) 174.

[18] E. Storm and H.I. Israel, Nucl. Data Tabl. A7 (1970) 565

[19] R.R. Kinsey, et. al., Proc. 9th Int. Symp. of Capture-Gamma-Ray Spectroscopy and Related Topics, 8-12 October 1996, Budapest, Hungary, in press.

[20] R.B. Firestone, Tables of Isotopes. CD ROM Edition, Wiley-Interscience, 1996.

[21] N.G. Gusev, P.P. Dmitrieev, Radioactive Chains: Handbook, 2d ed. Energoatomizdat, Moscow, 1988 (in Russian).

[22] S. Pearlstein, Astrophys. J. 346 (1989) 1049.

[23] K.K. Gudima, S.G. Mashnik and V.D. Toneev, Nucl. Phys. A 401 (1983) 329; JINR Communications P2-80-774 and P2-80-777, Dubna (1980).

[24] S.G. Mashnik, Izv. Akad. Nauk, Ser. Fiz. 60 (1996) 73 [Bull. Russian Ac. Sci.: Physics, 60 (1996) 58]; S.G. Mashnik, A.J. Sierk, O. Bersillon and T. Gabriel, Los Alamos National Laboratory Report LA-UR-97-2905 (1997); see also the Web page at: http://t2.lanl.gov/publications/publications.html.

[25] V.S. Barashenkov, Le Van Ngok, L.G. Levchuk, Zh.Zh. Musul'manbekov, A.N. Sosnin, V.D. Toneev and S.Yu. Shmakov, JINR Report R2-85-173, Dubna (1985); V.S. Barashenkov, F.G. Zheregi and Zh.Zh. Musul'manbekov, Yad. Fiz. 39 (1984) 1133 [Sov. J. Nucl. Phys. 39 (1984) 715]; V.S. Barashenkov, B.F. Kostenko and A.M. Zadorogny, Nucl. Phys. A 338 (1980) 413.

[26] G.A. Lobov, N.V. Stepanov, A.A. Sibirtsev and Yu.V. Trebukhovskii, ITEP Preprint ITEP-91, Moscow (1983); A.A. Sibirtsev, N.V. Stepanov and Yu.V. Trebukhovskii, ITEP Preprint ITEP-129, Moscow (1985); N.V. Stepanov, ITEP Preprint ITEP-81, Moscow (1987); N.V. Stepanov, ITEP Preprint ITEP-55-88, Moscow (1988) (in Russian).

[27] T.W. Armstrong and K.C. Chandler, Nucl. Sci. Eng. 49 (1972) 110 and references therein.

[28] R.E. Prael and H. Lichtenstein, Los Alamos National Laboratory Report LA-UR-89-3014 (1989); see also the Web page at: http://www-xdiv.lanl.gov/XTM/lcs/lahet-doc.html.

[29] P.G. Young, E.D. Arthur and M.B.Chadwick, Los Alamos National Laboratory Report LA-12343-MS (1992); M.B. Chadwick and P.G. Young, Phys. Rev. C 47 (1993) 2255.

[30] M. Blann, Phys. Rev. C 54 (1996) 1341.

[31] V.S. Barashenkov and V.D. Toneev, Interaction of High Energy Particles and Nuclei with Atomic Nuclei [in Russian] (Atomizdat, Moscow, 1972).

[32] V.S. Barashenkov, A.S. Iljinov, N.M. Sobolevskii, V.D. Toneev, Usp. Fiz. Nauk 109 (1973) 91 [Sov. Phys.-Usp. 16 (1973) 31].

[33] A.S. Iljinov, M.V. Kazarnovsky, E.Ya. Paryev, Intermediate-Energy Nuclear Physics (CRC Press, Boca Raton, Florida, 1994).

[34] H.W. Bertini and M.P. Guthrie, Nucl. Phys. A 169 (1971) 670; H.W. Bertini, Phys. Rev. 188 (1969) 1711 and references therein.

[35] K. Chen, Z. Frankel, G. Fridlandder, J.R. Grover, J.M. Miller and Y. Shimamoto, Phys. Rev. 166 (1968) 948; K. Chen, G. Ffiedlander, G.D. Harp and J.M. Miller, Phys. Rev. C 4 (1971) 2234.

[36] V.S. Barashenkov, H.W. Bertini, K. Chen, G. Friedlander, G.D. Harp, A.S. Iljinov, J.M. Miller, V.D. Toneev, Nucl. Phys. A 187 (1972) 531.

[37] K.K. Gudima, G.A. Ososkov, V.D. Toneev, Yad. Fiz. 21 (1975) 260 [Sov. J. Nucl. Phys. 21 (1975) 138].

[38] S.G. Mashnik and V.D. Toneev, JINR Communication P4-8417, Dubna (1974).

[39] S.G. Mashnik, A.J. Sierk, O. Bersillon and T. Gabriel, Los Alamos National Laboratory Report LA-UR-97-3176 (1997) and next paper in this issue, nucl-th/9709014.

[40] H.J. Krappe, J.R. Nix and A.J. Sierk, Phys. Rev. C 20 (1979) 992.

[41] A.G.W. Cameron, Can. J. Phys. 35 (1957) 1021.

[42] V.S. Barashenkov, A.S. Iljinov, V.D. Toneev, F.G. Gereghi, Nucl. Phys. A 206 (1973) 131.

[43] A.S. Iljinov, M.V. Mebel, N. Bianchi, E.De Sanctis, C. Guardalo, V. Lucherini, V. Muccifora, E, Polli, A.R. Reolon and P. Rossi, Nucl. Phys. A 543 (1992) 517.

[44] J.W. Truran, A.G.W. Cameron and E. Hilf, in: Proc. Int. Conf. on the Properties of Nuclei Far From the Region of Beta-Stability, Leysin, Switzerland, 1970, v. 1, p. 275.

[45] V.S. Barashenkov, A.S. Iljinov, V.D. Toneev and F.G. Gereghi, Nucl. Phys. A 222 (1974) 204.

[46] P. Fong, Statistical theory of nuclear fission (Gorgon and Breach Science Publishers, Ney York, 1969).

[47] W.A. Coleman and T.W. Armstrong, Nucl. Sci. Eng. 43 (1971) 353

[48] M.P. Guthrie, ORNL-TM-3119, Oak Ridge National Laboratory (1970).

[49] Radiation Scielding Information Center, "HETC Monte Carlo High-Energy Nucleon-Meson Transport Code", Report CCC-178, Oak Ridge National Laboratory (August 1977).

[50] Y. Yariv and Z. Frankel, Phys. Rev. C 20 (1979) 2227; Phys. Rev. C 24 (1981) 488.

[51] R.E. Prael and M. Bozoian, LA-UR-88-3238, Los Alamos National Laboratory (September 1988).

[52] J. Barish et al., "HETFIS High-Energy Nucleon Meson Transport Code with Fission," ORNL/TM-7882, Oak Ridge National Laboratory (1981); F.S. Alsmiller, R.G. Alsmiller, Jr., T.A. Gabriel, R.A. Lillie and J. Barish, Nucl. Sci. Eng. 79 (1981) 147.

[53] L. Dresner, "EVAP – A Fortran Program for Calculation the Evaporation of Various Particles from Excited Compound Nuclei", ORNL-TM-196, Oak Ridge National Laboratory (april 1962); P. Cloth, D. Filges, G. Sterzenbach, T.W. Armstrong and B.L. Colborn, "The KFA-Version of the High-Energy Transport Code HETC and the Generalized Evaluation Code SIMPEL", Kernforschungsanlage Jülich Report Jül-Spez-196, 1983.

[54] F. Atchinson "Spallation and Fission in Heavy Metal Nucley under Medium Energy Proton Bombardment", in: *Targets for Neutron Beam Spallation Sources*, Jül-Conf-34, Kernforschungsanlage Jülich GmbH (January 1980).

[55] M.B. Chadwick, P.G. Young, P. Oblozinski and A. Marcinkowski, Phys. Rev. C 49 (1994) R2885.

[56] M.V. Mebel, A.S. Iljinov, C. Grandi, G. Reffo and M. Blann, submitted Nucl. Inst. Meth. (1997); Proc. Int. Conf. Nucl. Data for Science and Tech., Trieste, Italy May, 1997.

Table 1
Approximation coefficients for the function $\sigma = \sum_{i=0}^{k} a_i E^i, \qquad (\sigma\,[mb], E\,[GeV])$

E	100-350 MeV k=4	350-800 MeV k=5	800-2600 MeV k=4
a_0	.16082579E+2	.91163994E+0	.10809485E+2
a_1	-.98011691E+2	.72710174E+2	.12760849E+1
a_2	.48105521E+2	-.22074848E+3	-.25036816E+1
a_3	-.92886532E+2	-25781415E+3	.10439362E+1
a_4	.63086480E+3	-.25781415E+3	-.13817290E+0
a_5		.77078179E+2	

Table 2
Experimental cumulative yields of the ground states of ^{209}Bi(p,x)–reaction products at E_p= 1500 MeV and 130 MeV

		E_p=1500MeV	E_p=130MeV
Nucleus	Half life	Cross Section [mb]	Cross Section [mb]
^{*207}Bi	32.2 y	58.0 ± 7.5	-
^{206}Bi	6.243 d	26.2 ± 3.2	88.1 ± 9.3
^{205}Bi	15.31 d	24.5 ± 2.9	109 ± 23
^{204}Bi	11.22 h	25.2 ± 3.0	97.0 ± 11.4
^{203}Bi	11.73 h	19.4 ± 2.5	107 ± 13
^{202}Bi	1.67 h	11.0 ± 2.2	138 ± 15
^{201}Bi	108 m		85.5 ± 11.7
^{200}Bi	36 m	8.4 ± 1.0	61.6 ± 8.0
^{203}Pb	51.837 h	44.3 ± 4.9	230 ± 35
^{201}Pb	9.33 h	29.9 ± 5.0	139 ± 17
^{200}Pb	21.5 h	28.4 ± 3.3	122 ± 14
^{199}Pb	90 m	30.7 ± 5.8	113 ± 23
^{198}Pb	2.4 h	25.0 ± 5.0	20.0 ± 8.2
^{201}Tl	72.912 h	38.7 ± 4.7	166 ± 27
^{200}Tl	26.1 h	36.2 ± 4.2	108 ± 13
^{199}Tl	7.42 h	32.9 ± 4.5	101 ± 18
^{198}Tl	5.3 h	27.4 ± 4.6	22.0 ± 3.7
^{197}Tl	2.84 h		13.4 ± 2.4
^{196}Tl	1.84 h		18.0 ± 5.3
^{194}Tl	33.0 m	11.4 ± 3.5	
^{203}Hg	46.612 d	1.15 ± 0.12	
^{195}Hg	9.9 h	12.6 ± 3.8	
^{192}Hg	4.85 h	23.4 ± 3.6	
^{198}Au	2.696 d	0.46 ± 0.18	
^{192}Au	4.94 h	30.6 ± 4.9	
^{191}Pt	2.9 d	20.2 ± 4.1	
^{188}Pt	10.2 d	25.1 ± 2.9	
^{188}Ir	41.5 h	24.7 ± 2.8	
^{186}Ir	15.8 h	10.2 ± 1.8	
^{184}Ir	3.02 h	16.4 ± 3.7	
^{*185}Os	93.6 d	29.3 ± 3.6	
^{182}Os	22.1h	23.4 ± 2.9	
^{183}Re	70.0 d	17.3 ± 2.9	
^{182}Re	12.7 h	26.3 ± 2.9	
^{181}Re	19.9 h	20.5 ± 4.5	
^{179}Re	19.7 m	16.4 ± 2.0	
^{176}Ta	8.08 h	22.6 ± 5.4	

Table 2 (continued)

		E_p=1500MeV	E_p=130MeV
Nucleus	Half life	Cross Section [mb]	Cross Section [mb]
^{174}Ta	1.18 h	15.6 ± 2.1	
^{173}Ta	3.14 h	16.8 ± 3.1	
^{172}Ta	36.8 m	6.6 ± 1.1	
^{173}Hf	23.6 h	25.6 ± 3.1	
^{*172}Hf	1.87 y	13.2 ± 1.5	
^{170}Hf	16.01 h	18.5 ± 2.6	
^{*173}Lu	1.37 y	23.2 ± 4.4	
^{171}Lu	8.24 d	22.4 ± 2.5	
^{169}Lu	34.06 d	16.2 ± 2.7	
^{166}Yb	56.7 h	11.1 ± 1.3	
^{160}Er	28.58 h	9.6 ± 1.1	
^{157}Dy	8.14 h	15.1 ± 1.8	
^{153}Tb	2.34 d	8.2 ± 1.1	
^{*153}Gd	241.6 d	2.7 ± 0.8	
^{151}Tb	17.609 d	7.9 ± 0.9	
^{149}Gd	9.4 d	8.3 ± 0.9	
^{147}Gd	38.1 h	6.6 ± 0.9	
^{146}Gd	48.27 d	6.1 ± 0.7	
^{147}Eu	24.0 d	9.5 ± 1.2	
^{146}Eu	4.59 d	6.7 ± 0.7	
^{145}Eu	5.93 h	3.8 ± 0.6	
^{*143}Pm	265 d	1.07 ± 0.35	
^{139}Ce	137.66 d	2.4 ± 0.4	
^{140}La	40.280 h	1.3 ± 0.2	
^{140}Ba	12.746 h	0.82 ± 0.11	
^{127}Xe	36.4 d	2.0 ± 0.2	
^{121}Te	17.78d	1.4 ± 0.3	
^{113}Sn	115.09 d	0.75 ± 0.12	
^{111}In	2.83 d	1.13 ± 0.15	
^{105}Rh	35.36 h	4.3 ± 0.5	
^{95}Tc	20.0 h	2.4 ± 0.5	
^{99}Mo	2.75 d	4.5 ± 0.6	
^{95}Nb	35.02 d	6.2 ± 0.9	
^{95}Zr	64.02 d	1.65 ± 0.21	
^{89}Zr	78.4 h	2.7 ± 0.4	
^{88}Zr	83.4 d	0.22 ± 0.03	
^{*88}Y	106.61 d	2.7 ± 0.5	
^{87}Y	80.3 h	4.4 ± 0.5	
^{85}Sr	64.08 d	5.2 ± 0.8	
^{83}Rb	86.2 d	4.5 ± 0.9	

Table 3
Experimental and simulated independent yields (in mb) of the ground states of ^{209}Bi(p,x)–reaction products at E_p= 1500 MeV and 130 MeV

				E_p=1500MeV					
Nucleus	Half life	Exp. cr. sec.	CEM95	LAHET	INUCL	HETC	CASCADE	ALICE	GNASH
^{206}Po	8.8 d	3.3±0.5	1.3	4.3	1.2	4.5	2.3		
^{202}Tl	12.23 d	4.8±0.7	4.8	4.6	8.6	7.3	3.1		
^{200}Tl	26.1 h	7.8±1.7	6.1	5.5	12.1	7.1	4.6		
^{146}Eu	4.59 d	0.59±0.12	0.41	5.1	0.15		0.07		
^{140}La	40.28 h	0.45±0.17		0.08					
^{*102}Rh	2.9 y	0.69±0.12		1.5	2.9				
^{95}Nb	35.02 d	3.8±0.5		1.2	5.8				
^{76}As	26.32 h	3.7±0.6		0.80	2.7				
^{74}As	17.77 d	2.1±0.3		1.7	2.5				
				E_p=130MeV					
^{207}Po	5.80 h	24.5±3.8	34.8	38.2	20.6	36.2	45.2	35.8	33.6
^{206}Po	8.8 d	44.6±11.9	39.1	47.2	28.0	38.2	68.5	58.2	32.1
^{205}Po	1.66 h	30.5±3.7	45.9	43.7	25.7	39.5	60.2	57.8	21.2
^{204}Po	3.53 h	43.1±5.2	45.2	56.3	22.5	47.2	85.6	72.8	25.5
^{203}Po	36.7 m	38.5±8.9	47.6	52.1	3.2	51.0	66.8	57.1	24.6
^{202}Po	44.7m	50.8±7.0	37.5	62.3	0.10	57.9	86.3	67.3	36.3
^{206}Bi	6.243 d	57.7±6.5	79.1	71.4	66.0	50.4	122.5	113.4	168.1
^{201}Pb	9.33 h	46.0±11.9	58.9	28.7	25.1	4.7	18.1	10.7	10.6
^{200}Tl	26.1 h	15.4±8.1	6.2	1.9	16.5	0.07	0.17	0.46	
^{198}Tl	5.3 h	4.0±3.0	2.5	1.4	18.8		0.47	0.96	

Table 4
Experimental and simulated independent and cumulative yields of metastable states of ^{209}Bi(p,x)–reaction products at E_p=1500 MeV and E_p=130 MeV

Nucleus	Half life	Yield	Experimental cross sec. [mb]	Calculation (GNASH) [mb]
E_p=1500MeV				
^{204m}Pb	67.2 m	ind	4.4±1.3	
^{202m}Pb	3.53 h	ind	14.0±2.1	
^{197m}Pb	44.6 m	cum	8.8±2.5	
^{196m}Tl	1.41 h	ind	15.9±3.2	
^{194m}Tl	32.8 m	ind	4.4±0.6	
^{193m}Hg	11.8 h	ind	9.9±1.4	
^{183m}Os	9.9 h	cum	11.8±1.8	
^{150m1}Tb	3.48 h	ind	4.4±1.0	
^{101m}Rh	4.34 d	cum	1.8±0.2	
^{90m}Y	3.19 h	ind	2.4±0.4	
^{82m}Rb	6.472 h	ind	2.5±0.4	
E_p=130MeV				
^{202m}Pb	3.53 h	ind	10.8±2.3	11.4
^{197m}Pb	44.6 m	cum	13.4±2.4	10.6

Table 5
Experimental total yields [mb] of the ground and metastable states of ^{209}Bi(p,x)–reaction products at E_p=1500 MeV

Nucleus	Half life	Yield	Exp. cr. sec.	CEM95	LAHET	INUCL	HETC	CASCADE
^{203}Pb	51.837 h	g+m1+m2	25.9±5.8	13.8	11.2	18.8	17.0	10.3
^{196}Au	6.183 d	g+m1+m2	0.80±0.13	1.6	0.93	2.4	0.22	1.2
^{194}Au	38.02 h	g+m1+m2	1.37±0.24	2.8	1.5	3.6	0.30	1.8
^{96}Tc	4.28 d	g+m	0.96±0.22		1.0	2.8		
^{82}Br	35.3 h	g+m	3.2±0.4		0.40	2.3		
^{*60}Co	5.2714 y	g+m	1.7±0.4		1.2	0.64		

Table 6
Statistics of simulation-to-experiment comparisons.

Code	E_p=130MeV N^{g+m}_{EXP}=30, N^{g}_{EXP}=28 $^{\star 1}$			E_p=1500MeV N^{g+m}_{EXP}=100, N^{g}_{EXP}=89 $^{\star 1}$		
	letter in Fig. 11	N_C/N_S	$\langle H \rangle$	letter in Fig. 12	N_C/N_S	$\langle H \rangle$
CEM95	A	23/28	1.73	A	49/64	1.95
INUCL	B	13/28 13/23$^{\star 2}$	11.1 2.59	B	54/86	2.95
CASCADE	C	22/28	2.89	C	50/64	1.83
HETC	D	19/26	3.22	D	41/62	2.64
LAHET(ISABEL)	E	24/28	1.86			
LAHET(Bertini)	F	23/28	1.85	E	63/89	2.51
ALICE	G	23/28	2.43			
GNASH	H	8/10	1.98			

$^{\star 1}$ N^{g+m}_{EXP} means number of all measured products, N^{g}_{EXP} means number of ground state measured products
$^{\star 2}$ with exception of ^{200}Bi, ^{201}Bi, ^{202}Bi, ^{202}Po, ^{203}Po

Figures Captions

Fig. 1. Plots of the recommended values of the monitor reaction excitation functions (A - ^{27}Al(p,x)^{24}Na, B - ^{27}Al(p,x)^{22}Na).

Fig. 2. A scheme of the extraction of the 800-2600 MeV external proton beam.

Fig. 3. A scheme of the extraction of the 70-200 MeV external proton beam.

Fig. 4. Relative distribution of the track numbers characterizing the background of secondaries near the extracted 1500 MeV and 130 MeV proton beams.

Fig. 5. The γ-spectra of the ^{209}Bi(p,x)–reaction products measured at proton energies of 1500 MeV and 130 MeV (the "cooling" times are 20 hours and 3.5 hours, respectively).

Fig. 6. Loading characteristics of the spectrometer.

Fig. 7. Characteristics of the spectrometer (A - effictiveness, B - height factor).

Fig. 8. Time depenedences of the ^{209}Bi (p,x)–reaction product decays at E_p=1500 MeV (A) and E_p=130 MeV (B).

Fig. 9. Product mass distribution of the ^{209}Bi(p,x)–reaction for E_p = 130 MeV.

Fig. 10. Product mass distribution of the ^{209}Bi(p,x)–reaction for E_p = 1500 MeV proton.

Fig. 11. Simulation-to-experiment ratios versus relative mass difference between an initial target nucleus and a particular product nucleus for E_p = 130 MeV. Letters are explained in Table 6.

Fig. 12. Simulation-to-experiment ratios versus relative mass difference between an initial target nucleus and a particular product nucleus for E_p = 1500 MeV. Letters are explained in Table 6.